Chinese Chemical Letters 32 (2021) 740–744

Contents lists available at ScienceDirect

Chinese Chemical Letters

journal homepage: www.elsevier.com/locate/cclet

Communication

# Quinoline-based aggregation-induced delayed fluorescence materials for highly efficient non-doped organic light-emitting diodes

Liang Zhang[a,b], Yin-Feng Wang[a,c], Meng Li[a], Qing-Yu Gao[b,*], Chuan-Feng Chen[a,c,*]

[a] Beijing National Laboratory for Molecular Sciences, CAS Key Laboratory of Molecular Recognition and Function, Institute of Chemistry, Chinese Academy of Sciences, Beijing 100190, China
[b] College of Chemical Engineering, China University of Mining and Technology, Xuzhou 221116, China
[c] University of Chinese Academy of Sciences, Beijing 100049, China

ARTICLE INFO

*Article history:*
Received 10 June 2020
Received in revised form 10 July 2020
Accepted 24 July 2020
Available online 26 July 2020

*Keywords:*
Quinoline
Aggregation-induced emission
Thermally activated delayed fluorescence
Non-doped organic light-emitting diode

ABSTRACT

Three new emitters, namely 10,10'-(quinoline-2,8-diyl)bis(10*H*-phenoxazine) (**Fene**), 10,10'-(quinoline-2,8-diyl)bis(10*H*-phenothiazine) (**Fens**) and 10,10'-(quinoline-2,8-diyl)bis(9,9-dimethyl-9,10-dihydroacridine) (**Yad**), featuring quinoline as a new electron acceptor have been designed and conveniently synthesized. These emitters possessed small singlet–triplet splitting energy ($\Delta E_{st}$) and twisted structures, which not only endowed them show thermally activated delayed fluorescence (TADF) properties but also afforded a remarkable aggregation-induced emission (AIE) feature. Moreover, they also showed aggregation-induced delayed fluorescence (AIDF) property and good photoluminescence (PL) property, which are the ideal emitters for non-doped organic light-emitting diodes (OLEDs). Furthermore, high-performance non-doped OLEDs based on **Fene**, **Fens** and **Yad** were achieved, and excellent maximum external quantum efficiencies ($EQE_{max}$) of 14.9%, 13.1% and 17.4%, respectively, were obtained. It was also found that all devices exhibited relatively low turn-on voltages ranging from 3.0 V to 3.2 V probably due to their twisted conformation and the AIDF properties. These results demonstrated the quinoline-based emitters could have a promising application in non-doped OLEDs.



Organic light-emitting diodes (OLEDs) have attracted much attention in academic and industrial communities owing to their low energy cost, high-quality color, light weight, rapid response and flexibility [1–4]. However, the traditional fluorescent emitters for OLEDs still require improvement in terms of their devices cannot exceed the theoretical maximum exciton utilization of 25%, according to the principle of conservation of spin [5–7]. Although phosphorescent OLEDs can fully utilize electrogenerated singlet and triplet excitons to provide high electroluminescence (EL) efficiency by utilizing precious-metal-based phosphorescent materials to increase spin-orbit coupling of singlet ($S_1$) state and triplet ($T_1$) state [8–11]. These phosphorescent materials are expensive for containing transition metals such as iridium and platinum [12–14], which can raise the manufacturing cost and limit their practical applications [15]. As the promising third-generation organic luminescent material after the conventional fluorescent and phosphorescent materials, purely organic materials with thermally activated delayed fluorescence (TADF) have attracted considerable attention due to their high exciton utilization efficiency [16–20].

TADF emitters for OLEDs have made great progress so far [21–25]. However, the development of high-performance OLED devices generally needed guest-host doping technique to alleviate concentration-caused emission quenching and exciton annihilation processes [26,27]. The doping technique requires complicated control of the doping concentration [28] and the reproducibility of OLED device is cumbersome as well [29–32]. Owing to their rigid structures and special properties, heterocyclic compounds have been widely utilized as acceptors for TADF materials, which included pyrimidine [33], heptazine [34], quinoxzline [35], phenanthroline [36], triazine [37,38], pyrazine [39,40], dibenzo[a,j]phenazine [41] and naphthyridine [42]. Among different kinds of heterocycles, quinoline derivatives stand out as important molecules with a wide range of interesting pharmacological activity and unique physicochemical property. However, there have been no reports quinoline-based TADF emitters and their applications in OLEDs so far. Herein, we report three emitters **Fene**, **Fens** and **Yad** with quinoline as a new electron acceptor. These emitters have strong intramolecular interactions, which can cause

* Corresponding authors.
*E-mail addresses:* gaoqy@cumt.edu.cn (Q.-Y. Gao), cchen@iccas.ac.cn (C.-F. Chen).

https://doi.org/10.1016/j.cclet.2020.07.041
1001-8417/

stable excited state configuration and restrict aggregation-caused quenching (ACQ) effect. Consequently, the emitters exhibited aggregation-induced emission (AIE) and aggregation-induced delayed fluorescence (AIDF) properties, and highly efficient non-doped OLEDs based on **Fene**, **Fens** and **Yad** achieved high maximum EQEs of 14.9%, 13.1% and 17.4%, respectively.

The synthetic routes of **Fene**, **Fens** and **Yad** were shown in Scheme 1. According to the literature procedure [43], 8-bromo-2-chloroquinoline was prepared. Then, compounds **Fene**, **Fens** and **Yad** were conveniently synthesized in good yields by palladium-catalyzed cross-coupling reactions of 8-bromo-2-chloroquinoline with 9,9-dimethyl-acridan, phenothiazine and phenoxazine, respectively. The target compounds were purified *via* column chromatography and temperature-gradient sublimation with high vacuum conditions. Their structures were confirmed by $^{1}$H NMR, $^{13}$C NMR, HRMS spectra and single-crystal X-ray structures.

Single crystals of emitters **Fene**, **Fens** and **Yad** suitable for X-ray diffraction analyses were obtained from their solution in $CH_2Cl_2$/petroleum ether. As depicted in Fig. 1, the torsion angles of **Fene** between the two phenoxazine units and the quinoline moiety are 106.31° and 30.98°, respectively. The twisted molecular structure could be helpful for separating its highest occupied molecular orbitals (HOMO) and lowest unoccupied molecular orbitals (LUMO), resulting in small $\Delta E_{ST}$. Moreover, the twisted conformation of **Fene** could also weaken the intermolecular interactions, which would greatly suppress concentration-caused emission quenching. Similarly, it was found that the torsion angles between the two phenothiazine units and the quinoline moiety in **Fens** are 159.63° and 72.86°, and the torsion angles between the two acridine units and the quinoline moiety in **Yad** are 171.84° and 75.51°. Compound **Fene** existed strong multiple intramolecular interactions with the distances from 2.83 Å to 3.21 Å between the donor and the acceptor. Similarly, it was also found that there existed the multiple interactions between the donor and the acceptor of **Fens** with the distances from 2.95 Å to 3.20 Å, and the multiple $\pi$-$\pi$ interactions between the donor and the acceptor of **Yad** with the distances from 2.87 Å to 3.24 Å. These multiple interactions could be helpful to rigidify the molecular structures and greatly suppress the exciton annihilation.

In order to predict the performance of these luminogens, the spatial distributions of the highest occupied molecular orbitals (HOMOs) and lowest unoccupied molecular orbitals (LUMOs) of **Fene**, **Fens** and **Yad** were calculated by density functional theory (DFT) using the B3LYP function with the 6−31 G(d) basis set. As shown in Fig. 2, it was found that the LUMOs of the three emitters were mainly distributed in the acceptor moieties, and the HOMOs of **Fene**, **Fens** and **Yad** were mainly distributed in the donor moieties. These molecules showed highly twisted structures due to the larger steric hindrance. The HOMO/LUMO energy levels were calculated to be −5.03/−2.08 eV for **Fene**, −4.97/−1.86 eV for **Fens** and −5.19/−2.14 eV for **Yad**, respectively. The excited state features of **Fene**, **Fens** and **Yad** were further calculated based on the time-dependent DFT using the B3LYP function with the 6−31 G(d) basis set, respectively. The $S_1/T_1$ values were calculated to be −2.24/−2.23 eV for **Fene**, −2.50/−2.52 eV for **Fens** and −2.54/−2.56 eV

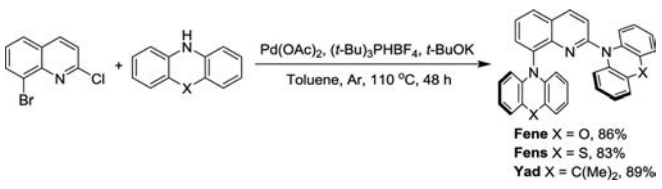


**Scheme 1.** Synthesis of emitters **Fene**, **Fens** and **Yad**.

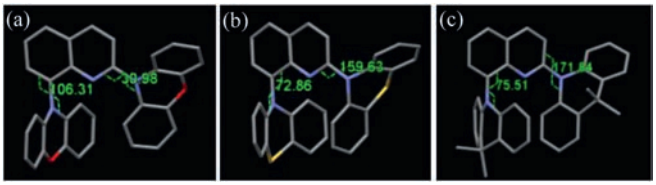


**Fig. 1.** The torsion angles of (a) **Fene**, (b) **Fens** and (c) **Yad**.

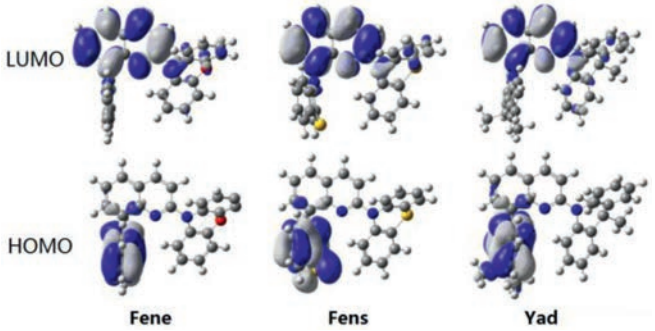


**Fig. 2.** The HOMO and LUMO of **Fene**, **Fens** and **Yad** obtained by the Gaussian 09 DFT B3LYP/6-31+G* level of theory.

for **Yad**, which gave the $\Delta E_{ST}$ values of 0.01, 0.02 and 0.02 eV for **Fene**, **Fens** and **Yad**, respectively. Obvious spatial separation between the HOMOs and LUMOs and the small $\Delta E_{ST}$ demonstrated that the reverse intersystem crossing (RISC) processes of $T_1$ to $S_1$ could be activated by the thermal energy of room-temperature.

The UV–vis spectra of **Fene**, **Fens** and **Yad** were measured in toluene with the concentration of $10^{-5}$ mol/L. As depicted in Fig. S7a (Supporting information), these emitters exhibited similar absorption bands due to their similar D-A-D structures and donor units. The absorption band in the range of 287–318 nm could be assigned to the locally excited (LE) transitions of the acridine, phenothiazine and phenoxazine moieties or the quinoline unit. Moreover, the lower energy absorptions ranging from 357 nm to 377 nm corresponded to the strong intramolecular charge-transfer (ICT) transitions from different donor units to quinoline moiety. Furthermore, the fluorescence spectra of **Fene**, **Fens** and **Yad** exhibited obvious solvatochromism effect. As shown in Fig. S8 (Supporting information), the solvatochromic effect resulted in the red-shifted emission with increased solvent polarity, indicating the emission features of ICT for the emitters. The emission bands of **Fene**, **Fens** and **Yad** centered at 584, 591 and 544 nm, and their absolute PLQYs in neat films were 58.24%, 36.11% and 79.63%, respectively.

To obtain their experimental $\Delta E_{ST}$ values, we investigated the emission spectra of **Fene**, **Fens** and **Yad** in films at 77 K. Their fluorescence bands at 77 K were centered at 566, 563 and 543 nm, which resulted in $S_1$ energy levels of 2.19, 2.20 and 2.28 eV, respectively. Moreover, it was also found the phosphorescence bands of **Fene**, **Fens** and **Yad** were centered at 576, 570 and 552 nm (Table S4 in Supporting information), and their corresponding $T_1$ energy levels were 2.15, 2.17 and 2.24 eV, respectively. Thus, the $\Delta E_{ST}$ values were estimated to be 0.04 eV for **Fene**, 0.03 eV for **Fens** and 0.04 eV for **Yad**. Small $\Delta E_{ST}$ could enable an efficient RISC process with a thermal aid for these compounds. In order to confirm the emission feature of **Fene**, **Fens** and **Yad**, transient PL spectra were also measured in neat films. As shown in Fig. 3, these emitters displayed the delayed fluorescence (DF) components with lifetimes of 2.75, 3.27 and 16.05 μs, respectively, which might be

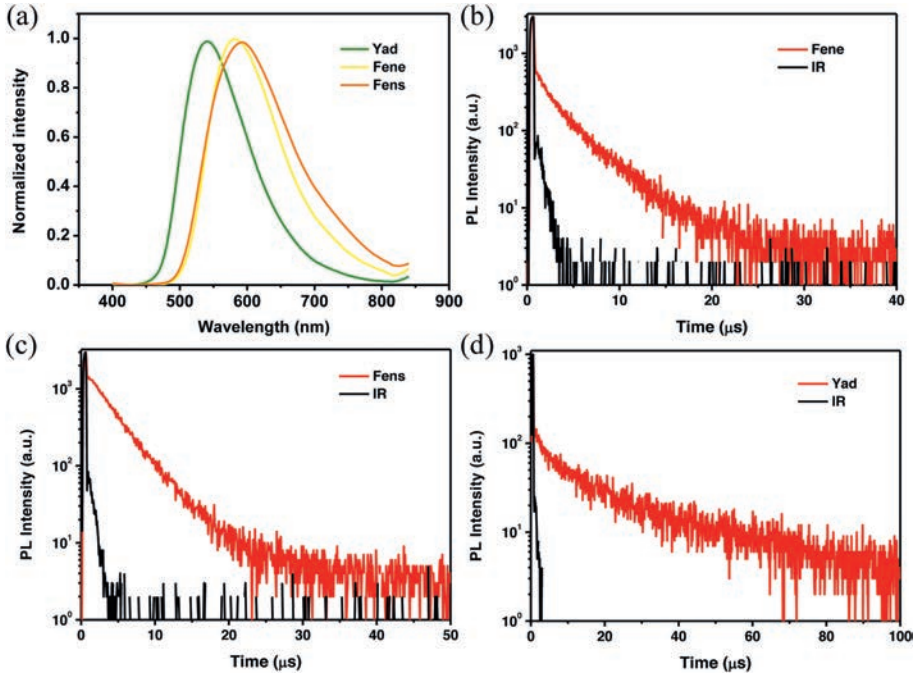


**Fig. 3.** (a) Fluorescence spectra of **Fene**, **Fens** and **Yad** in neat films at room temperature; Transient PL spectra of (b) **Fene**, (c) **Fens** and (d) **Yad** in neat films at room temperature.

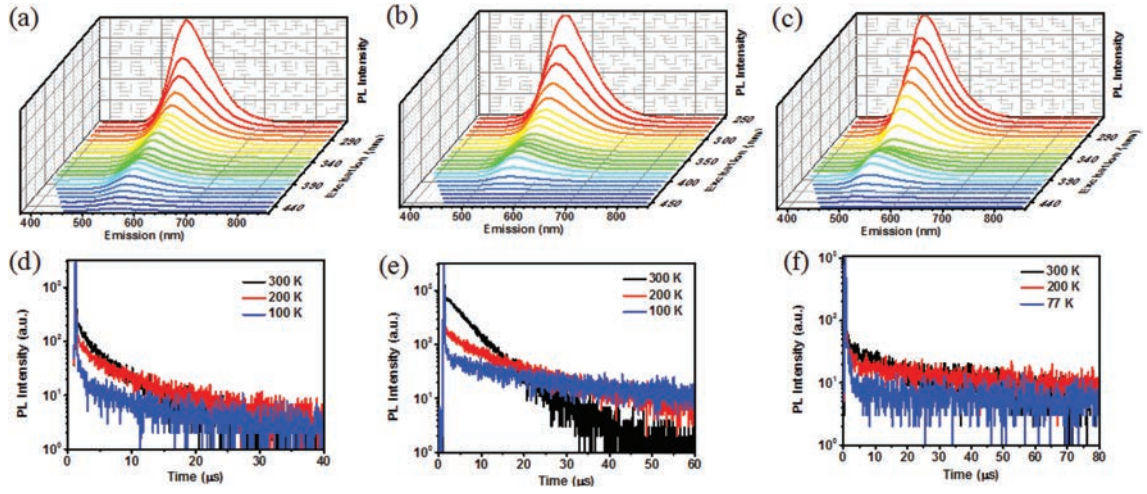


**Fig. 4.** Steady-state excitation-emission mapping of (a) **Fene**, (b) **Fens** and (c) **Yad** in neat films at room temperature; the temperature-dependent transient photoluminescence spectra of (d) **Fene**, (e) **Fens** and (f) **Yad** in the neat films.

due to the thermal up-conversion of excitons from $T_1$ to $S_1$. Moreover, the temperature-dependent transient PL of **Fene**, **Fens** and **Yad** (Fig. 4) was then investigated. The ratio of the delayed component gradually increased from 77 K to 300 K, demonstrating the typical characteristics of TADF for these emitters. Excitation-emission fluorescence mappings of **Fene**, **Fens** and **Yad** were also carried out in neat films. It was further found that fluorescence intensity weakened with increasing excitation wavelength.

Thermogravimetric analyses (TGA) were also carried out to investigate the thermal stability of the emitters. As shown in Figs. S4–S6 (Supporting information), **Fene**, **Fens** and **Yad** exhibited good thermal stability with a 5% weight loss decomposition temperature ($T_d$) of 360, 320 and 314 °C, respectively. These results indicated that these luminogens possessed adequate thermal stability for the light-emitting devices.

Cyclic voltammetry (CV) was further used to investigate the electrochemical properties of the emitters. As shown in Fig. S7 (Supporting information), according to the onsets of oxidation and reduction potentials in their CV curves, the HOMO/LUMO levels of **Fene**, **Fens** and **Yad** were determined to be -5.90/-3.04 eV, -5.63/-2.53 eV and -6.09/-3.29 eV, respectively. These favorable HOMO/LUMO levels matched well with the widely used hole transporting material of 1,1-bis[(di-4-tolylamino)phenyl]cyclohexane (TAPC) and electron-transporting layer of 1,3,5-tri(mpyrid-3-yl-phenyl) benzene (TmPyPB), which could facilitate the charge carrier injection and transportation from adjacent layer to the emissive layer.

The PL spectra of emitters **Fene**, **Fens** and **Yad** in THF/water mixtures were measured to investigate their AIE properties. As shown in Fig. 5, the PL spectra of **Fene**, **Fens** and **Yad** showed

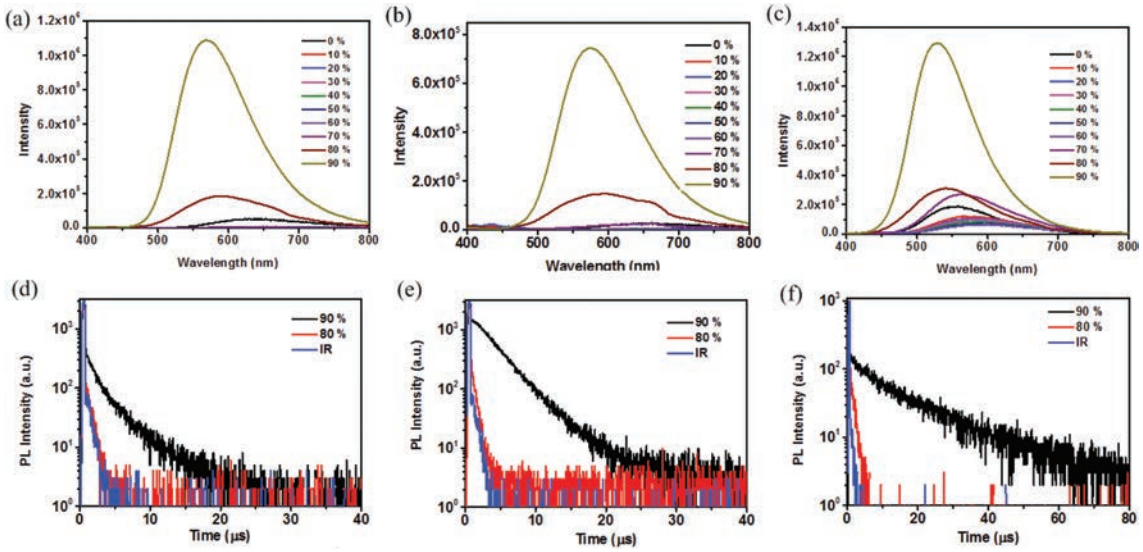


**Fig. 5.** PL spectra of (a) **Fene**, (b) **Fens** and (c) **Yad** in THF/water mixtures with different water fractions (fw); PL decay curves of (d) **Fene**, (e) **Fens** and (f) **Yad** in THF/water mixtures with different water fractions (fw) in air.

negligible emission in dilute THF solution. However, when the value of water fraction reached to 80%, relatively strong fluorescence emissions were observed. With the continuing increase of water fraction, the fluorescence intensities enhanced gradually. When the value of water fraction reached to 90%, the fluorescence intensities of **Fene**, **Fens** and **Yad** were much stronger than those in THF, suggesting that the typical AIE characteristics existed. The transient PL curves of **Fene**, **Fens** and **Yad** were also measured in THF under air atmosphere at room temperature. Interestingly, when the water fraction varied from 80% to 90% in THF-water mixtures, the lifetimes and proportion of DF gradually increased with the increase of water fractions under air atmosphere at room temperature. Rotations of the aromatic rings and vibrations of **Fene**, **Fens** and **Yad** resulted in the conformational changes and thus influenced the RISC processes with the loss of DF in solution under air atmosphere. Long-lived luminescence under air atmosphere indicated that the triplet excited states in aggregate states

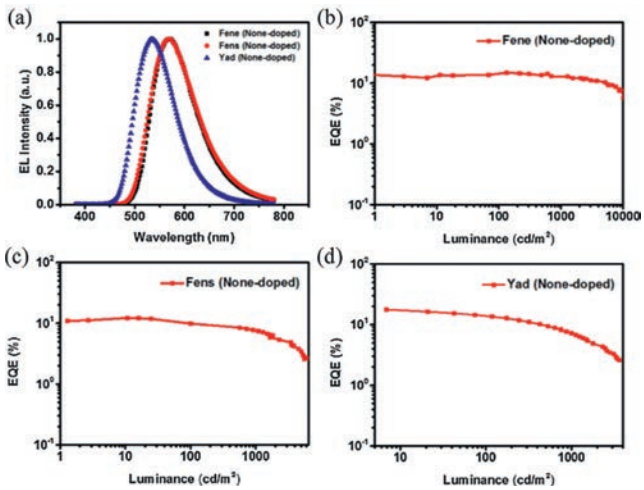


**Fig. 6.** (a) Electroluminescence spectra of devices at 6 V; external quantum efficiency versus luminance curves for the devices of (b) **Fene**, (c) **Fens** and (d) **Yad**.

**Table 1**
Summary of EL data for the devices.

| Emitter | Host (wt%) | $V_{on}$[a] (V) | $CE_{max}$ [cd/A] | $PE_{max}$ (lm/W) | $EQE_{max}$ (%) | EL peak[b] (nm) |
|---|---|---|---|---|---|---|
| **Fene** | None-doped | 3.2 | 42.2 | 31.57 | 14.9 | 570 |
| **Fens** | None-doped | 3.2 | 36.8 | 30.40 | 13.1 | 568 |
| **Yad** | None-doped | 3 | 58.14 | 57.01 | 17.4 | 534 |

$CE_{max}$: maximum current efficiency; $PE_{max}$: maximum power efficiency; $EQE_{max}$: maximum external quantum efficiency.
[a] The turn-on voltage recorded at a brightness of 1 cd/m$^2$.
[b] The main EL emission peak at a driving voltage of 6 V.

were protected from oxygen, consequently leading to the effective RISC and delayed fluorescence emission. The outstanding emission characteristics of these materials could make them to have the great potential application as emitters in non-doped OLEDs. Thus, as shown in Fig. 6, the devices were fabricated with the structure of indium tin oxide (ITO)/(TAPC) (30 nm)/4,4′,4″-tri(*N*-carbazolyl)-triphenylamine (TCTA) (5 nm)/emission (15 nm)/(TmPyPB) (65 nm)/LiF (1 nm)/Al (100 nm), in which TAPC and TmPyPB were used as hole- and electron-transportation layers, respectively. Moreover, TCTA was inserted between TAPC and the emitting layer to reduce the hole-injection barrier and achieve step-by-step increments for each energy level. We further used LiF served as the electron-injection layer to eliminate the barrier caused by the interface electric double layer and reduce the Fermi level of the cathode. The non-doped OLEDs were fabricated by using co-deposited films of emission layers. As shown in Table 1, the non-doped optimal devices based on **Fene**, **Fens** and **Yad** displayed the maximum EL emissions at 570, 568 and 534 nm, respectively. Moreover, the non-doped devices of **Fene**, **Fens** and **Yad** showed excellent performances with the $EQE_{max}$ of 14.9%, 13.1% and 17.4%, respectively. It was also found that the turn-on voltages of the non-doped devices are all low ranging from 3.0 V to 3.2 V.

In summary, we have conveniently synthesized three emitters **Fene**, **Fens** and **Yad** with quinoline as the new electron acceptor, which exhibited both TADF and AIE properties. Small $\Delta E_{ST}$ and twisted structures made them show good photoluminescence and AIDF properties, which could be greatly benefit for highly efficient

non-doped OLEDs. Consequently, non-doped OLEDs based on the emitters were fabricated, which achieved excellent $EQE_{max}$ of 14.9% and 13.1% with neat films of **Fene** and **Fens**, respectively. Moreover, the non-doped device based on the **Yad** neat film achieved the $EQE_{max}$ of 17.4% owing to the good photoluminescence and obvious AIDF property. Notably, all devices exhibited relatively low turn-on voltages ranging from 3 V to 3.2 V. This represents the first highly efficient TADF emitters based on the quinoline electron acceptor. The results presented herein also suggested that the quinoline-based emitters could have a potential application in non-doped OLEDs for displays and solid-state lighting.

## Declaration of competing interest

We declare that we have no known competing financial interests or personal relationships that could have appeared to influence the work reported in this paper.

## Acknowledgment

We thank the National Natural Science Foundation of China (Nos. 91956119, 21871272, 21521002) for financial supports.

## Appendix A. Supplementary data

Supplementary material related to this article can be found, in the online version, at doi:https://doi.org/10.1016/j.cclet.2020.07.041.

## References

[1] H. Uoyama, K. Goushi, K. Shizu, et al., Nature 492 (2012) 234–238.
[2] Q. Zhang, B. Li, S. Huang, et al., Nat. Photonics 8 (2014) 326–332.
[3] Z. Yang, Z. Mao, Z. Xie, et al., Chem. Soc. Rev. 46 (2017) 915–1016.
[4] T. Huang, W. Jiang, L. Duan, J. Mater. Chem. C 6 (2018) 5577–5596.
[5] Y. Liu, C. Li, Z. Ren, et al., Nat. Rev. Mater. 4 (2018) 18020.
[6] J. Luo, S. Gong, Y. Gu, et al., J. Mater. Chem. C 4 (2016) 2442–2446.
[7] Y. Wang, Yu. Zhang, W. Hu, et al., ACS Appl. Mater. Interfaces 11 (2019) 26165–26173.
[8] P. Wei, D. Zhang, L. Duan, Adv. Funct. Mater. 29 (2019) 1907083.
[9] M. Li, Y. Liu, R. Duan, et al., Angew. Chem. Int. Ed. 56 (2017) 8818–8822.
[10] H. Liu, J. Zeng, J. Guo, et al., Angew. Chem. Int. Ed. 57 (2018) 9290–9294.
[11] D.H. Ahn, H. Lee, S.W. Kim, et al., ACS Appl. Mater. Interfaces 11 (2019) 14909–14916.
[12] F. Song, Z. Xu, Q. Zhang, et al., Adv. Funct. Mater. 28 (2018) 1800051.
[13] M. Li, Y.F. Wang, D. Zhang, et al., Angew. Chem. Int. Ed. 59 (2020) 3500–3504.
[14] Y. Zhang, X. Zhang, H. Zhang, et al., J. Phys. Chem. C 123 (2019) 24746–24753.
[15] W. Li, B. Li, X. Cai, et al., Angew. Chem. Int. Ed. 58 (2019) 11301–11305.
[16] L.S. Cui, Y.L. Deng, D.P.K. Tsang, et al., Adv. Mater. 28 (2016) 7620–7625.
[17] D. Zhang, X. Song, M. Cai, et al., Adv. Mater. 30 (2018) 1705406.
[18] W. Chen, F. Song, Chin. Chem. Lett. 30 (2019) 1717–1730.
[19] M. Cai, D. Zhang, J. Xu, et al., ACS Appl. Mater. Interfaces 11 (2019) 1096–1108.
[20] Y.F. Wang, H.Y. Lu, C. Chen, et al., Org. Electron. 70 (2019) 71–77.
[21] D. Zhang, M. Cai, Y. Zhang, et al., Mater. Horiz. 3 (2016) 145–151.
[22] D.W. Zhang, M. Li, C.F. Chen, Chem. Soc. Rev. 49 (2020) 1331–1343.
[23] Z.G. Wu, H.B. Han, Z.P. Yan, et al., Adv. Mater. 31 (2019) 1900524.
[24] X. Chen, J.W. Zhao, X.H. Zheng, et al., Chin. Chem. Lett. 30 (2019) 1989–1993.
[25] W. Yuan, H. Yang, M. Zhang, et al., Chin. Chem. Lett. 30 (2019) 1955–1958.
[26] C. Li, R.S. Nobuyasu, Y. Wang, et al., Adv. Opt. Mater. 5 (2017) 1700435.
[27] M. Zhang, L. Chen, X. Xu, et al., J. Mater. Chem. C 7 (2019) 9850–9855.
[28] J. Guo, Z. Zhao, B.Z. Tang, Adv. Opt. Mater. 6 (2018) 1800264.
[29] J. Huang, H. Nie, J. Zeng, et al., Angew. Chem. Int. Ed. 56 (2017) 12971–12973.
[30] Z. Huang, Z. Bin, R. Su, et al., Angew. Chem. Int. Ed. 59 (2020) 9992–9996.
[31] J. Guo, X.L. Li, H. Nie, et al., Chem. Mater. 29 (2017) 3623–3631.
[32] J. Guo, Z. Zhao, B.Z. Tang, Adv. Opt. Mater. 6 (2018) 1800264.
[33] R. Komatsu, H. Sasabe, Y. Seino, et al., J. Mater. Chem. C 4 (2016) 2274–2278.
[34] J. Li, T. Nakagawa, J. MacDonald, et al., Adv. Mater. 25 (2013) 3319–3323.
[35] K. Shizu, H. Tanaka, M. Uejima, et al., J. Phys. Chem. C 119 (2015) 1291–1297.
[36] K. Wu, T. Zhang, L. Zhan, et al., Adv. Opt. Mater. 4 (2016) 1558–1566.
[37] A. Endo, K. Sato, K. Yoshimura, et al., Appl. Phys. Lett. 98 (2011) 083302.
[38] Y.F. Wang, H.Y. Lu, Y.F. Shen, et al., Chem. Commun. 55 (2019) 9559–9562.
[39] K. Kawasumi, T. Wu, T. Zhu, et al., J. Am. Chem. Soc. 137 (2015) 11908–11911.
[40] S. Wang, X. Yan, Z. Cheng, et al., Angew. Chem. Int. Ed. 54 (2015) 13068–13072.
[41] P. Data, P. Pander, M. Okazaki, et al., Angew. Chem. Int. Ed. 55 (2016) 5739.
[42] C. Chen, H.Y. Lu, Y.F. Wang, et al., J. Mater. Chem. C 7 (2019) 4673–4680.
[43] F. Cottet, M. Marull, O. Lefebvre, et al., Eur. J. Org. Chem. 8 (2003) 1559–1568.